Measurements of Local Two-Phase Flow Parameters in a Boiling Flow Channel

Byong Jo YUN*, Goon-Cherl PARK

Seoul National University, Department of Nuclear Engineering,
Sinlim dong 56-1, Seoul 151-742, Korea.
Tel: +82-2-880-7210, Fax: +82-2-889-2688, E-mail: parkgc@plaza.snu.ac.kr

Chul Hwa SONG, Moon Ki CHUNG

Korea Atomic Energy Research Institute, Thermal Hydraulics Team,
Yusung P.O. Box 105, Taejon 305-600, Korea.
Tel: +82-42-868-8876, Fax: +82-42-868-8362, E-mail: chsong@nanum.kaeri.re.kr

ABSTRACT

Local two-phase flow parameters were measured to investigate the internal flow structures of steam-water boiling flow in an annulus channel. Two kinds of measuring methods for local two-phase flow parameters were investigated. These are a two-conductivity probe for local vapor parameters and a Pitot tube for local liquid parameters. Using these probes, the local distribution of phasic velocities, interfacial area concentration (IAC) and void fraction is measured. In this study, the maximum local void fraction in subcooled boiling condition is observed around the heating rod and the local void fraction is smoothly decreased from the surface of a heating rod to the channel center without any wall void peaking, which was observed in air-water experiments. The distributions of local IAC and bubble frequency coincide with those of local void fraction for a given area-averaged void fraction.

* Present address: Korea Atomic Energy Research Institute, Thermal Hydraulics Team.

1. INTRODUCTION

During several decades, two-phase flow phenomena have been studied with theoretical and experimental methods for engineering applications in nuclear thermal hydraulics and other related industries. In particular, precise prediction of phasic behaviors in subchannels under two-phase flow conditions is of great importance to the safety analysis of nuclear power plants and the verification of thermal-hydraulic design code.

The measurements of distributions of local two-phase flow parameters are needed to get detailed information on the flow structure of two-phase flow. But the measurements of local phasic parameters in two-phase flow are very difficult since most of currently available instrumentations can be applied to rather limited conditions and the phasic behaviors are so complicated to understand.

For a few decades, a considerable amount of works on the measurements of local two-phase flow parameters has been successfully performed by many investigators since Neal & Bankoff (1963)'s work on the measurement

of local void profile in an air-water flow condition. Serizawa (1974) measured the turbulence structure of air-water bubbly flow, Kataoka et al. (1984) measured local IAC in air-water bubbly flow, Welle (1985) measured local two-phase flow parameters in air-water flow, Sim & Lahey (1986) measured phase distributions in a complex flow channel. Through these experimental works, the flow structure of air-water two-phase flow was figured out, and prediction of the phase distribution in air-water flow condition was satisfactorily achievable.

Since most of these works were, however, limited to adiabatic flow conditions like air-water flow, so more comprehensive understanding on the two-phase flow phenomena is required to predict these local flow parameters in boiling flow situations. Especially, measurements of the distribution of local flow parameters are essentially needed since they could give us detailed information on the flow structures of boiling flow.

The present work is an experimental study on the measurements of local phasic parameters in a steam-water boiling flow. For this, an annular boiling channel was set up and the measuring techniques for local phasic parameters were investigated. The instrumentations developed in the present work are a two-conductivity probe for local vapor parameters and a Pitot tube for local liquid parameter, both of which are applicable to steam-water boiling flow conditions. By applying these techniques, the local distribution of void fraction, phasic velocities, vapor turbulent fluctuation and IAC were measured simultaneously in a steam-water boiling flow. The system pressure and liquid superficial velocity in the test channel are about 1.5 *bar* and less than 2 *m/sec*, respectively, and the flow regime considered is limited to the subcooled boiling.

2. EXPERIMENTAL SETUP

The boiling loop is composed, as shown in Fig. 1, of a test channel, a cooler, a pump and a preheater. The test channel is designed to be of an annular type, that is, a circular stainless steel tube of 33 *mm* I.D. inside which a heating rod with 16 *mm* O.D. is located. The test channel is 2 *m* in length and the flow area of the test channel is 6.54 cm^2. Transparent glass tube of 30 *cm* in height is installed in the test channel so that visual observation or taking photographs are possible. The maximum heat generation rate of a heating rod is 30 *kW* and it can be controlled by a thyristor chip. The local probes are located 1.6 *m* downstream of the inlet of the test channel (L/D_h = 94). The heated part of the heating rod is 1.7 *m* in length and the unheated part is located 0.1 *m* downstream of the measuring position. Distilled water is delivered as a cooling water. The outer wall of the test channel is thermally insulated with ceramic wool. A traversing system to position local probes in the flow channel consists of a ball slide unit and a micro-vernier meter with the spatial resolution of 1/100 *mm*.

3. MEASURING METHODS

3.1 Two-Conductivity Probe Method

Radial distributions of local parameters of vapor phase such as phasic velocity, interfacial area concentration (IAC) and void fraction are measured by a two-conductivity probe method in this study. The conductivity probe method is basically based on the difference of electrical resistance between vapor and liquid phases. It was developed first by Neal & Bankoff (1963). And then Serizawa (1974), Herringe & Davis (1976) and Welle (1985) extended it to a two-conductivity probe method for measuring local gas-phase parameters such as local void fraction, bubble velocity, bubble frequency and bubble diameter in air-water flow conditions. Ishii (1975) proposed a new mathematical theory to get the local IAC using local probes such as two-conductivity probe and optical probe. Local IAC can be determined by measuring both the interfacial velocity and the surface direction at that point. However, measurement of the surface direction of a bubble is practically impossible without some mathematical modellings.

Kataoka et al. (1984) suggested a practical measuring method to get local IAC by a two-conductivity probe, and observed that the velocity fluctuations due to turbulences of bubble are significant in actual measurements. They proposed a good statistical model by considering the turbulent fluctuations of velocity components of bubbles in all three directions. Later, Kataoka et al. (1994) developed a multi-probe method to

consider the turbulent fluctuations of three-dimensional velocity components of bubbles. However, application of the probe is limited to relatively large bubbles and large diameter channel due to its complex geometry. And thus, in this study, the two-conductivity probe method was adopted to use due to its simplicity.

The two-conductivity probe used in this study is schematically shown in Fig. 2. The sensing element is made of a teflon-coated stainless steel wire of 0.127 *mm* O.D. and it is sharpened to form a conical shape at the probe tip. The distance between two probe tips should be properly selected by considering the bubble motion and the sampling rate of A/D converter. If a probe distance is too long, bubbles which pass through the front probe may be disturbed so as not to contact the end probe. If it is too short, the measurement accuracy of vapor velocity is not so good due to limitation of sampling rate of A/D converter. Many previous investigators reported that the most suitable distance between two probe tips is about 5 *mm*. However, more attention should be paid to determine a proper probe distance in case of steam-water boiling flow conditions because bubbles can be generated or grown up on the surface of a heating rod in a distance between two probe tips. In this study, it was found out, from analyses of high-speed photograph, that the probe distance of 3 to 5 *mm* is appropriate for this boiling flow condition. The probe distance was measured with an electron microscope with a spatial resolution of 1/1000 *mm*.

Instantaneous measurements of the changes in local resistivity in a two-phase flow stream are converted into a voltage drop between a probe tip and the ground. Two kinds of electrical circuit were tested for this study: one is a D.C circuit named a bridge amplifier circuit and the other is a A.C rectifier circuit. It is well known that the polarizing phenomena happen around a sensing tip if D.C power is applied to the probe. In a series of preliminary experiments in our air-water and steam-water flow conditions, however, the decrease of bubble frequency caused by the polarization phenomenon was not observed, but the corrosion around a stainless steel sensing tip was observed. In particular, the probe degradation caused by corrosion was serious at high temperature conditions of steam-water boiling flow than in air-water flow. The lifetime of a probe was about 2 *hours* in steam-water flow and 2 *weeks* in air-water flow. The corrosion problem could be resolved by adopting a A.C rectifier circuit, which was modified from the circuit used in the measurements of film thickness in wavy flow by Kang (1992).

Determination of the Cutoff Level for Phase Discrimination

The determination of a proper cutoff level, which indicates the boundary between the two phases, is very important for getting accurate measurements of void fraction and bubble velocities. Many previous researchers, such as Neal & Bankoff (1963), Herringe & Davis (1974) and Serizawa (1974), used the Schmitt triggering circuit or computer algorithms with a preset constant cutoff level for all bubbles. But this preset cutoff level is not always proper because the output signal can be varied by probe fouling, flow condition and change of water conductivity. Especially, the multi-peaked output signal above the preset level, which can be caused by a chaotic motion of bubbles, coalescence of bubbles or wetting of the probe tips, affects the measurement of bubble frequency. To overcome this drawback, some researchers developed new methods to get accurate two-phase flow parameters. Liu (1989) developed a new iterative algorithm. He performed the phase discrimination by comparing with the channel-averaged void fractions obtained by a quick closing method in a air-water flow. The algorithm is based on the combination of pulse height and slope conditions. But it is difficult to apply this algorithm to steam-water boiling flow condition. Thus, in this study, a new computer algorithm was developed for the phase discrimination of steam-water boiling flow by a two-conductivity probe.

The new algorithm is based on the pulse height and slope criteria as by previous investigators. The difference is such that the cutoff level for each bubble is different from one case to another. The cutoff level is calculated based on the slope criterion as well as the pulse height, which can be varied for each bubble, instead of a constant value of preset cutoff level for all bubbles. Hence, the cutoff level for each bubble is proportional to the pulse height produced by individual bubble. But the phase discrimination for signals above the cutoff level is carried out by the slope condition. The proportional constant is predetermined by air-water experiments. The proportional constant is found to be 0.55 by comparison of the global void fractions measured in the pre-tests of air-water flow. In this test, the global void fraction is

measured by a quick closing method. The flow conditions of the experiments are less than 40 % of area-averaged void fraction and 3 *m/sec* of bubble velocity. Typical variation of local void fraction in a circular channel with various proportional constants is shown in Fig. 3. As shown in this figure, the change of local void fraction due to change of the proportional constant is small. The change of area-averaged void fractions due to change of proportional constants is also shown in Fig. 4. From these figures, it is shown that the change of area-averaged void fraction due to change of the proportional constant is very small for all cutoff levels, which indicates that the present algorithm of phase discrimination is reliable enough to provide good data.

Herringe & Davis (1974) also reported that the area-averaged void fraction is not very sensitive to changes in proportional constants. But, the void fraction was very sensitive in the range of less than 10 % and larger than 80 % of trigger levels. They adopted a single cutoff level for whole pulse heights. The main advantage of the present algorithm is such that the cutoff level for each bubble is varied with the signal variations induced by the afore-mentioned factors. The algorithm is based on the fact that the pulse heights of the output signals can be different for all bubbles. In previous investigations, if a pulse height is lower than the preset level, the pulse is, in general, neglected in the calculation of local parameters even though it is explicitly generated by a bubble. But the present algorithm will identify the signal as a bubble. From the pre-tests, the present algorithm was proven to show good agreements with measured global void fraction in air-water conditions. The flow chart of the present algorithm for the phase discrimination is described in detail in Fig. 5, and a comparison of a raw signal with the signal converted by the algorithm is typically shown in Fig. 6.

Estimation of Local Vapor Parameters

The local void fraction is defined as the fraction of bubble elapsed time to the total measuring time at a local position. For statistical treatments of local void fraction, the total measuring time should be sufficiently long. Figure 7 shows typical changes of local void fraction with the total measuring time. The local void fraction is nearly constant after about 20 *sec* of integration time. In this study, the total measuring time for each local position is set to about 1~2 *minutes*, which is long enough to satisfy the repeatability of void fraction. Fig. 8 shows a typical distribution of local void fractions from the front and end probes. The local void fraction obtained at two probes coincides well with each other. The void fraction is determined by the upstream signal of the two-conductivity probe, that is, the signal from the front probe because the signal from the end probe may be affected by the wake of bubbles which pass through the front probe. The local bubble frequency, defined as the number of bubbles that pass through a measuring point per unit time, is also measured by the front probe, and it is used in the estimation of local IAC.

The local vapor velocity, more exactly, the interfacial phasic velocity, can be calculated based on the elapsed time at the boundaries between vapor and liquid phases, if it is assumed that all bubbles move with a uni-directional motion and a bubble hitting the front probe will sequently hit the end probe. The local vapor velocity (V_b) can be calculated, if the mean elapsed time (τ) is known, as follows;

$$V_b = \Delta Z / \tau, \qquad (1)$$

where ΔZ is a distance between the front and end probes.

A bubble hitting the front probe, in general, will not always pass through the end probe. Thus, it is necessary to validate whether the signals from both probes correspond to the same bubble or not. This is not always the case, since there are bubbles that are cut by the front probe and then deviate from the main flow direction and thus miss the end probe, or others that are only cut by the end probe. Hence, identification of signals are performed by comparing the chordal lengths measured by both the front and end probes. If a chordal length measured by the end probe is within $\pm$ 30 % compared to that by the front probe, then the signal from the end probe is considered to come from the same bubble to generate that of the front probe.

Bubble velocity spectrum at each measuring point is evaluated from by Eq. (1) and the local mean velocity is calculated arithmetically from the spectrum. And the velocity fluctuation, that is, the turbulent fluctuation of a bubble is also obtained by calculating the standard deviation of bubble velocities.

In the formulation of two-fluid model, IAC appears in the interfacial transfer terms, which are the most important ones in the two-fluid model. These terms are, however, not properly considered in mixture models such as the slip model and drift-flux model. Many previous researchers tried to measure the IAC. Most of previous studies on the IAC are, however, limited to adiabatic two-phase flow conditions, and currently available data are also limited to the global IAC such as area-averaged or volume-averaged ones. In this study, local IAC and Sauter mean diameter are measured to give detailed information on the flow structure of boiling flow.

The local IAC is estimated using the methodology of Kataoka et al. (1984). They derived the expression of the local IAC, by assuming that the bubbles are spherical and every part of the bubbles has the same probability of being intersected by the probe, as follows;

$$a_i(r) = \frac{4N_i\left\{\sum_j \frac{1}{|v_{gj}|} / (\sum)\right\}}{1-\cot\frac{\alpha_o}{2}\ln\left(\cos\frac{\alpha_o}{2}\right)-\tan\frac{\alpha_o}{2}\ln\left(\sin\frac{\alpha_o}{2}\right)} \quad (2)$$

where

$$\frac{\sin 2\alpha_o}{2\alpha_o} = \frac{1-(\sigma_z^2/\overline{|v_{gz}|^2})}{1+3(\sigma_z^2/\overline{|v_{gz}|^2})} \quad (3)$$

$$\sigma_z = (\sum_j N_{gj}\cdot(v_{gj}-v_{gz})^2/\sum_j N_{gj})^{1/2} \quad (4)$$

Using Eq.s (2), (3) and (4), the local IAC can be calculated by measuring the local vapor velocity spectrum and bubble frequency at each measuring point. These can be applied to the forced subcooled boiling regimes where small bubbles can be considered to move mainly in axial direction and the lateral motion must be very small in an average sense.

The Sauter mean diameter is calculated to analyze the IAC. The reason why the Sauter mean diameter is the most important length scale in the analysis of IAC comes from the fact that the definition of Sauter mean diameter is similar to that of IAC. The local Sauter mean diameter (D_s) can be calculated, by assuming that the bubble shape is spherical, as follows;

$$D_s = \frac{6\alpha}{a_i} \quad (5)$$

More recently, Kalkach et al. (1993) proposed a new methodology for measuring local IAC using a local probe. The methodology allows us to directly measure the average bubble size and bubble number density, which can not be done in Kataoka et al. (1984) methodology. They reported that this methodology gives good results in bubbly flow. It was pointed out, however, that the measured IAC provides unrealistic results if the methodology is applied to bubbly/slug transitional flow regime. In the present study, the Kataoka's methodology was adopted to use because the flow regime considered in this study is limited to the subcooled boiling regime and the method is appropriate to determine local phasic parameters at a real time basis.

Verification of Void Fraction and Vapor Velocity

Local void fraction is verified by separate air-water experiments in a glass tube of 8 *mm* I.D. Area-averaged void fraction is measured by a quick closing method. The flow conditions of the test loop are 0.5~3 *m/sec* of liquid velocity and 1.9~42.4 *%* of area-averaged void fraction. The mean relative error and standard deviation of the area-averaged void fraction are 5.6 *%* and 1.0 *%*, respectively.

Verification of the vapor velocity was carried out by the analysis of the high-speed photograph. The high-speed camera (PHOTEC) with a maximum shutter speed of 10000 *frames/sec* is used for this analysis. The shutter speed is set to 4000 *frames/sec* in experiments. The mean relative error and standard deviation of the local bubble velocity are 3.3 % and 3.1%, respectively.

3.2 Pitot Tube Method

The local liquid velocity in the boiling channel is measured by a Pitot tube to obtain information of internal flow structure and to identify the dependency of local superficial velocity (j_l) on other local two-phase flow parameters. The Pitot tube has been widely used in the local measurements of air and liquid velocities. The local fluid velocity can be obtained by measuring the dynamic pressure, that is, the difference between the stagnation pressure and static pressure at a local position. Most of the application was, however, limited to the single phase flow conditions. Anderson & Mantwouranis (1960) first measured the local liquid velocity in a two-phase flow. They suggested the

following equation for the calculation of liquid velocity in the two-phase flow;

$$\Delta P = \frac{1}{2}[\alpha \rho_g u_g^2 + J(1-\alpha)\rho_l u_l^2] \quad (6)$$

If a dispersed phase follows a streamline of the continuous phase at the probe tip, then the momentum exchange factor (J) becomes 1. If, on the other hand, the dispersed phase is brought completely to rest at the probe tip, then (J) value becomes 2. The first case is achieved approximately for gas bubbles in a liquid flow, the latter case for liquid droplets in a gas flow. (Reimann et al., 1983) In practical applications of Eq. (6), it can be assumed that the local phasic velocities are the same as each other or the gas momentum flux ($\alpha \rho_g u_g^2$) is negligible. The former assumption will be valid in high pressure steam-water flow conditions and the latter will be valid in low void fraction regions under low pressure condition.

Previous investigations such as Neal & Bankoff (1965), Malnes (1966), Bosio & Malnes (1969), Walmet & Staub (1969), Delhaye & Chevrier (1969), and Sim & Lahey (1986) used a Pitot tube to measure local liquid velocity in a bubbly flow. The data reduction model developed for local liquid velocity in two-phase flow are summarized in Table 1. (see Reimann et al., 1983)

The problems encountered when using a Pitot tube in two-phase flow conditions are such that bubbles can inflow into the Pitot tube and the flow field may be disturbed by the probe. To avoid the former problem, the pressure holes of the Pitot tube and the amount of volume exchange between pressure tube and sensor cell caused by pressure fluctuations of two-phase stream should be small. The latter problem can be minimized by adopting a small size of Pitot tube. In this study, a 1/16" Pitot tube (UNITED SENSOR) is used. The dynamic pressure of the Pitot tube is measured by a differential pressure transducer (VALIDYNE DP-103 with CD-15 demodulator), which is a diaphragm-exchangeable type. These instruments minimize the possibility of the problems of bubble inflow and disturbance of flow field. In this study, the cold water injection system is also used to remove the gas or vapor entrapped in the Pitot tube.

The calibration of the Pitot tube was carried out in the air-water annulus loop. A total of 17 sets of experiments, 12 sets in the single-phase flow and 5 sets in the air-water two-phase flow, were performed. The single-phase experiments were carried out to measure the momentum transfer factor (K), defined by:

$$\Delta P = K\frac{1}{2}\rho V^2 \quad (7)$$

The measurements of the momentum transfer factor (K) is requisite for local measurements in low velocity region because the drag force at the Pitot tube tip can be changed rapidly with the liquid velocity.

In air-water two-phase flow, the local liquid velocity can be calculated using various suggested models in Table 1. The accuracy of these models used to calculate local liquid velocity could not be fully investigated, even though a global continuity check was performed in this study. Among them, the Bosio & Malnes (1969) model showed good agreement with the average liquid velocities obtained by volume measurements. The mean relative error is 2.6 % in the air-water two-phase flow. A global continuity check was also performed using all the data obtained in this steam-water boiling flow. Among them, Neal & Bankoff (1965) and Reimann et al. (1981) models gave the mean relative errors of greater than 20 % and the other models gave the errors of less than 3.5 % in steam-water boiling flow. The mean relative error of the Bosio & Malnes model is 3.2 %.

The final form of the Bosio & Malnes (1969) model, which include a single-phase momentum transfer factor, is expressed as follows:

$$v_L = \frac{1}{\sqrt{1-\alpha^2/2}}\sqrt{\frac{2\Delta p}{K\rho_L}} \quad (8)$$

3.3 Two-Phase Flow Monitoring System

A large amount of memory and time are required, in general, to treat the raw data obtained from the two-conductivity probe and Pitot tube. In this study, a real-time data analysis software, VOID, was developed for the convenience of data processing as well as immediately visualizing both the experimental results and the status of the test loop. It has a capability of calculating various two-phase flow parameters and test

conditions. The calculated parameters are displayed at the monitor and stored into the mass storage of a IBM-PC (486-66MHz) during experiments. The calculation of bubble-related parameters for one acquisition takes about 1 *sec* and the acquisition is repeated for fifty times at each local measuring position.

4. RESULTS AND DISCUSSION

Measurements were performed with varying the heat flux, inlet subcooling and liquid flow conditions. A total of 37 sets of experiments were carried out in the subcooled boiling regime. Each experimental set covers twelve radial locations for local void fraction along the cross-section. The local liquid velocity around a heating rod was, however, not measured due to the size of the Pitot tube, and thus the local liquid velocity is measured at eleven positions along the cross-section. A summary of the experimental conditions is described in Table 2.

4.1 Distribution of Local Void Fraction and Bubble Frequency

In air-water flow, the interfacial transfer terms such as the interfacial mass and energy transfer are negligible because there exists no phase change and the difference of temperature between phases is negligible. In case of boiling flow, however, these terms could not be neglected due to the phase change phenomena, and the distribution of two-phase flow parameters should be thoroughly dealt with, especially in view of these interfacial transfer phenomena. Among these parameters, local void fraction is one of the most important parameters because it reflects the energy of the fluid and its distribution affects the distribution of other local parameters such as vapor velocity, liquid velocity and local IAC.

In air-water experiments, the so-called wall peaking of local void fraction was reported by many investigators. It has been known that the phenomena happen due to the migration of bubbles toward the wall, and thereby bubble frequency profile is similar to that of local void fraction. The lift force plays a great role in the transverse migration of bubbles. The nature of the lift force is not fully understood yet. Up to now, however, the lift force is known to be generated by a bubble rotation and shear flow in the continuous phase. Especially, a significant lift force can be generated by rotation of a small bubble at high flow condition. However, the wall peaking caused by the lift force was not observed in this steam-water boiling experiments.

The radial profile of local void fraction for various flow conditions and area-averaged void fraction is shown in Fig. 9. In the figure, $(r-R_{inner})/(R_{outer}-R_{inner})$ = 1 means the inner surface of the flow channel wall and $(r-R_{inner})/(R_{outer}-R_{inner})$ = 0 means the surface of the heating rod in the annulus channel. As shown in this figure, the local void fraction at all flow conditions is smoothly decreasing from the surface of the heating rod to the outer wall. This distribution of local void fraction is quite different from that of air-water experiments performed by other investigators where the wall void peaking were observed. In this study, the distribution of fluid temperature was not measured and thus the local distribution of fluid enthalpy can not be directly measured. However, the distribution in the bubble boundary layer can be calculated if the steam table is used. That is, the local distribution of fluid enthalpy is obtained using the saturation enthalpies of steam and liquid and the static quality at each point in the bubble boundary layer. The enthalpy distribution of single-phase core, however, can not be obtained. Jiji & Clark (1964) studied experimentally on the bubble boundary layer and single-phase liquid core. They reported that the temperature at the interface between single-phase core and bubble boundary layer approaches the inlet temperature as the heat flux is increased, and is generally well below the saturation temperature. And thus, the enthalpy distribution of single-phase liquid core can be presumed as a constant with inlet fluid enthalpy.

The radial void distribution coincides well with that of local enthalpy in the bubble boundary layer of the boiling channel. From the observation of high-speed photographs, the bubble boundary layer could be well distinguished from the single-phase core located near the outer wall of the annulus. However, small size of bubbles were sometimes observed in the highly subcooled region of the single-phase core. These bubbles come out stochastically from the bubble boundary layer by transverse motion. In general, the thickness of the bubble boundary layer decreases as the inlet subcooling and mass flux increase, and it increases as the heat flux increases. However, in this experiments, it was not so much dependent on the degree of inlet subcooling and liquid flow rate, but more dependent on the area-average void fraction. It may be due to the low degree of inlet subcooling of this experiments. As shown in Fig. 9,

it can be confirmed that the thickness of the bubble boundary layer has a similar value, irrespective of liquid mass flux, for the same value of area-averaged void fraction.

To obtain more precise information on the internal structures of boiling flow, the distribution of bubble frequency should be also known. The radial profile of local vapor bubble frequencies is shown in Fig. 10. The profiles show the trends similar to those of local void fraction, which indicates the fact that the bubble frequency is high in a region where the local void fraction is high, as shown in the figure. It was also observed that the increase of local void fraction caused by the increase of enthalpy is not due to the increase of vapor bubble size, but mainly due to the increase of vapor bubble frequency for a given area averaged void fraction in the subcooled boiling regime.

4.2 Distribution of Local Phasic Velocity

The local bubble and liquid velocities were measured simultaneously by a two-conductivity probe and a Pitot tube, respectively. It is usually known that the vapor velocity is greater than the liquid velocity due to the buoyancy force caused by the density difference between phases. And the slip velocity at low liquid flow condition is larger than that of high flow condition and the distribution of local phasic velocities is affected by the phase distribution in a channel. The radial profiles of local phasic velocities for vapor and liquid phases at various flow conditions are shown in Fig.s 11 and 12, respectively.

As shown in Fig. 11, the vapor velocity at the center of the channel is, in general, higher than those near the heating rod surface. But a sudden increase of bubble velocity near the heating rod was observed at the low flow conditions such as $\langle j \rangle$ = 047~0.49 *m/sec*, even though such an increase of bubble velocity was not observed at the higher flow conditions. In the bubble boundary layer near the heated surface, the buoyancy effect of bubbles ejected from a heating surface is relatively larger than that in high liquid flow condition, which is suppressed by the sufficient liquid in high flow conditions. Further investigation, however, is needed to comprehensively understand this phenomenon observed in the annulus boiling channel.

Figure 12 shows the profile of local liquid velocity. In case of single-phase flow, the velocity profile is parabolic along the radial direction due to the effect of shear force at the channel wall. In case of two-phase flow, however, the nonuniformity of void distribution and bubble velocity across the cross section of the test section causes the liquid velocity profile to deviate from that in single-phase liquid flow. At low flow conditions, the liquid velocity in the high void region of the bubble boundary layer increases when compared to that of single-phase liquid flow. It is due to the fact that the bubble with high velocity lifts the liquid phase with low velocity. However, the profile of liquid velocity resembles with that in single-phase liquid flow as liquid flow increases. In the flow condition of $\langle j \rangle$ = 1.67~1.76 *m/sec*, the profile of liquid velocity shows the trend similar to that in single-phase liquid flow. In this high flow condition, the change of liquid velocity around the heating rod due to the existence of bubbles is negligible, which indicates the fact that the slip velocity around the heating rod is very small.

The radial profile of the local slip velocity is shown in Fig. 13. The profile is similar to that of the vapor bubble velocity. The local slip velocity at the channel center is higher than that around the heating rod. It increases as the area-averaged void fraction increases for a given liquid flow condition and decreases as the area-averaged liquid superficial velocity is increased. The reason for the tendency of varying with liquid flow condition is such that the increase of vapor bubble velocity driven by the buoyancy force is suppressed by the increase of the liquid flow.

It is interesting to note that the local slip velocity near the heating rod at high flow conditions such as $\langle j \rangle$ = 1.67~1.76 *m/sec* is negative, which means that the liquid velocity is faster than vapor bubble velocity. Main reason for that observation comes from the effect of wall shear stress of liquid phase and from the fact that the velocity of some bubbles around the heating rod does not reach the terminal velocity at high flow condition. Especially, the bubbles detached from the boiling site of the heating rod will be accelerated from stagnant and this causes the bubble velocity spectrum to have lower mean value of bubble velocity.

The radial profile of the turbulent intensity of vapor bubble at various flow conditions and area-averaged void fraction is shown in Fig. 14. The relative turbulent fluctuations of vapor bubbles decrease from the surface of the heating rod to the channel center. Increase in area-averaged void fraction causes to increase the relative velocity fluctuation of vapor bubble for a given flow condition, whereas the increase of area-averaged liquid

superficial velocity decreases the relative velocity fluctuations of the vapor bubbles, which indicates that the relative velocity fluctuation of bubble is suppressed by the increase of liquid flow.

4.3 Distribution of Local IAC and Sauter Diameter

IAC is one of the most important parameters in the two-fluid model. To analyze the local IAC, the bubble size should be considered simultaneously with it, since the local void fraction is the product of bubble number density and the volume of a bubble. The radial distribution of the local IAC and Sauter mean diameter is shown in Fig.s 15 and 16, respectively.

As can be seen in Fig. 15, the radial distribution of local IAC has a trend similar to that of local void fraction for a given area-averaged void fraction. This means that the occurrence of bubble coalescence due to the increase of local void fraction is not so significant as discussed in previous secsion. The evidence for this phenomena is shown explicitly by comparison of the distribution of vapor bubble frequency, as shown in Fig. 10, and that of local Sauter mean diameter in Fig. 16. The bubble frequency distribution has the same trend as that of local void fraction as the local IAC distribution does. In addition, the variation of the order of the Sauter mean diameter is smaller than that of the vapor bubble frequency for a given area-averaged void fraction. This gives us some important insights on the development of the experimental correlation of the IAC.

These results imply explicitly that the most dominant reason for the increase of local IAC with the increase of local void fraction is due to the increase of bubble frequency for the same area-averaged void fraction in case of steam-water boiling flow. This was also observed in air-water experiment of previous investigators such as Kataoka & Serizawa (1990). They investigated the bubble size effect on the local IAC using the bubble size controlling technique at the channel entrance, and reported that the bubble frequency and bubble size are determined by the type of bubble generation system and so the local IAC also depends on the bubble size and bubble frequency at the channel entrance. In case of steam-water boiling flow, however, the bubble frequency and bubble size are determined by the enthalpy distribution, instability of bubble motion, liquid turbulent dissipation and fluid properties in a test channel. As shown in Fig. 16, the local Sauter diameter depends weakly on the area-averaged liquid superficial velocity, but mostly on the area-averaged void fraction as the local IAC does. It implies that the local Sauter diameter can be treated as a constant for a given area-averaged void fraction.

It should be noted, from Fig. 16, that the measured Sauter mean diameter of certain bubbles are larger than the channel gap size (8.5 *mm*) for $\langle j_f \rangle$ = 0.48 *m/sec*. It is due to the assumptions used in the calculation of IAC, such that turbulent fluctuation of a bubble velocity is approximately isotropic and the bubble shape is spherical. It seemed that these assumptions are not valid in the region of high void fraction ($\sim$ 10 %) and low liquid flow rate ($\sim$ 0.48 *m/sec*). The flow regime at this condition is a bubbly-to-slug transition regime. That is, in these experimental conditions, the bubble shape is not spherical and the turbulent fluctuations of x- and y- directions also should be measured simultaneously to get accurate value of the Sauter mean diameter and local IAC. In the analysis of high-speed photograph, some elongated bubbles, of which the axial length is greater than 10 *mm*, were observed in the bubble boundary layer.

5. SUMMARY AND CONCLUSION

The two-conductivity probe and Pitot tube methods are applied to the steam-water flow boiling in an annular channel to measure local flow parameters such as phasic velocity, interfacial area concentration and void fraction. Major findings in this study can be summarized as follows:

(1) In the two-conductivity probe method for measuring the local flow parameters in vapor phase, a new cutoff algorithm was successfully developed for the phase discrimination of steam-water boiling flow. And in the Pitot tube method, which was applied to boiling two-phase flow condition, the local liquid velocities were calculated successfully by modifying the Bosio & Malnes model.

(2) The void fraction decreases from the surface of the heating rod to the outer wall in subcooled boiling without any wall peaking, which was observed in air-water experiments. And the increase of local void fraction is mainly due to the increase of vapor bubble frequency for a given area-averaged void fraction in the subcooled boiling regime.

(3) Vapor velocities at the channel center are higher

than those near the channel wall region. But sudden decreases of vapor velocity around the heating rod were observed in low flow conditions. And the profiles of liquid velocity are parabolic and the location of maximum velocity of liquid phase moves toward the heating rod as the average void fraction increases in the low flow condition. In the flow condition of $\langle j_l \rangle$ = 1.67~1.76 *m/sec*, the profile of liquid velocity shows the trend similar to that in single-phase liquid flow.

(4) The profile of relative turbulent fluctuations of vapor bubbles, local IAC and bubble frequency show the trend similar to that of local void fraction.

NOMENCLATURE

$a_i(r)$	: local interfacial area concentration [*1/m*]
D_h	: hydraulic diameter [*m*]
D_s	: local Sauter diameter [*m*]
j_k	: superficial velocity of phase-*k* [*m/sec*]
K	: momentum transfer factor of the Pitot tube in a single-phase flow
L	: channel length [*m*]
N_{sv_j}	: number of bubbles at velocity, v_{sv_j}
N_t	: bubble numbers per second
V_b	: vapor bubble velocity [*m/sec*]
v_{sv_j}	: velocity measured by a two-conductivity probe [*m/sec*]
v_{sv}	: arithmetic mean of v_{sv_j}
v_L	: local liquid velocity [*m/sec*]
α	: local void fraction
ρ_g, ρ_l	: phasic density of vapor and liquid [kg/m^3]
Δp	: dynamic pressure measured by the Pitot tube
$\langle \phi \rangle$	: area-average of parameter, ϕ

REFERENCES

Herringe, R.A. and Davis, M.R., 1976, "Structural Development of Gas-Liquid Mixture Flows", *J. Fluid Mech.*, Vol. 73, part 1, pp. 97-123.

Ishii, M, 1975, Thermo-Fluid Dynamic Theory of Two-Phase Flow, Eyrolles, Paris.

Jiji, L.M. and Clark, J.A., 1964, "Bubble Boundary Layer and Temperature Profiles for Forced Convection Boiling in Channel flow", *Trans. ASME, J. of Heat Transfer*, pp. 50-58.

Kalkach-Navaro, Lahey, R.T., Jr., Drew, D.A. and Meyber, R., 1993, "Interfacial Area Density, Mean Radius and Number Density Measurements in Bubbly Two-Phase Flow", *Nuc. Eng. & Des.*, Vol. 142, pp. 341-351.

Kang, H.C, 1992, "A Study of Interfacial Structure and Film Condensation in a Stratified Flow," Ph.D. Thesis, Pohang Institute of Science and Technology, Pohang, Korea.

Kataoka, I., Ishii, M. and Serizawa, A., 1984, "Local Formulation of Interfacial Area Concentration and Its Measurements in Two-Phase Flow", NUREG/CR-4029.

Kataoka, I. and Serizawa, A., 1990, "Interfacial Area Concentration in Bubbly Flow", *Nuc. Eng. & Des.*, Vol. 120, pp. 163-180.

Kataoka, I., Ishii, M. and Serizawa, A., 1994, "Sensitivity Analysis of Bubble and Probe Geometry on the Measurements of Interfacial Area Concentration Gas-Liquid Two-Phase Flow", *Nuc. Eng. & Des.*, Vol. 146, pp. 53-69.

Liu, T.J., 1989, "Experimental Investigation of Turbulence Structure in Two-Phase Bubbly Flow," Ph.D. Thesis, Northwestern University.

Nasso, G.P., 1963, "Development of an Electrical Resistivity Probe for Void Fraction Measurements in Air-Water Flow," ANL-6738.

Herringe, R.A. and Davis, M.R., 1976, "Structural Development of Gas-Liquid Mixture Flows", *J. Fluid Mech.*, Vol. 73, part 1, pp. 97-123.

Neal, L.G. and Bankoff, S.G., 1963, "A High Resolution Resistivity Probe for Determination of Local Void Properties in Gas-Liquid Flow," *AIChE J.*, pp. 490-494.

Neal, L.G. and Bankoff, S.G., 1965, "Local Parameters in Cocurrent Mercury-Nitrogen Flow," *AIChE J*, pp. 624-635.

Reimann, J., Kusterer, H. and John, H., 1983, "Two-Phase Mass Flow Rate Measurements with Pitot Tubes and Density Measurements," Measuring Techniques in Gas-Liquid Two-Phase Flows, Symposium, Nancy, France, July 5-8.

Serizawa, A., et. al, 1974, "Turbulence Structures of Air-Water Bubbly Flow", *Int. J. MultiPhase Flow*, Vol. 2, pp. 221-233.

Sim, S.K. and Lahey, R.T., Jr., 1986, "Measurement of Phase Distribution in a Triangular Conduit," *Int. J. Multiphase Flow*, Vol. 12, No. 3, pp. 405-425.

Walmet, G.E. and Staub, F.W., 1969, "Pressure, Temperature and Void Fraction Measurement in Non-equilibrium Two-Phase Flow," Two-Phase Flow Instrumentation, pp. 89-101.

Welle, R.V., 1985, "Void Fraction, Bubble Velocity and Bubble Size in Two Phase Flow," *Int. J. Multiphase Flow*, Vol. 11, pp. 317-345.

Table 1. Data Reduction Model for Liquid Velocity by Pitot Tube. (Reimann et al., 1983)

Adoni (1961)	$v_L = \frac{1}{\sqrt{(1-\alpha^2)}} \sqrt{\frac{2\Delta p}{\rho_L}}$
Neal & Bankoff (1965)	$v_L = \frac{1}{\sqrt{2(1-\alpha)}} \sqrt{\frac{2\Delta p}{\rho_L}}$
Malnes (1966)	$v_L = \frac{1}{\sqrt{(1-\alpha)}} \sqrt{\frac{2\Delta p}{\rho_L}}$
Walmet & Staub (1969)	$v_L = \frac{1}{\sqrt{(1-\alpha)(1+\alpha/2)}} \sqrt{\frac{2\Delta p}{\rho_L}}$
Delhaye & Chevrier (1969)	$v_L = \sqrt{\frac{2\Delta p}{\rho_L}}$
Bosio & Malnes (1969)	$v_L = \frac{1}{\sqrt{1-\alpha^2/2}} \sqrt{\frac{2\Delta p}{\rho_L}}$
Reimann et al. (1981)	$v_L = \frac{1}{\sqrt{(1-\alpha)(1.5+0.5\tanh(6(\alpha-1/2)))}} \sqrt{\frac{2\Delta p}{\rho_L}}$

Table 2 Experimental Conditions

$\langle \alpha \rangle$	Pressure (psia)	$\langle j_g \rangle$ (m/sec)	$\langle j_l \rangle$ (m/sec)	Inlet subcooling (°C)
0.0138	20.4	0.022	1.76	10.1
0.0155	19.9	0.025	1.75	8.3
0.0288	20.2	0.048	1.67	6.6
0.0370	20.3	0.064	1.69	10.4
0.0383	20.1	0.066	1.69	9.6
0.0389	20.9	0.069	1.69	8.6
0.0451	20.4	0.078	1.67	8.8
0.0579	21.3	0.106	1.74	4.3
0.0594	20.1	0.107	1.71	5.8
0.0762	20.4	0.138	1.68	3.3
0.0000	-	0.000	1.76	-
0.0067	23.3	0.007	1.12	32.2
0.0109	23.2	0.013	1.11	31.7
0.0212	23.1	0.026	1.10	31.1
0.0271	23.2	0.034	1.09	31.1
0.0411	23.3	0.054	1.08	30.9
0.0719	23.1	0.101	1.06	29.6
0.0198	20.4	0.023	1.15	19.5
0.0491	20.2	0.062	1.14	20.6
0.0856	20.5	0.113	1.10	18.3
0.1034	20.0	0.149	1.04	24.5
0.0000	-	0.000	1.12	-
0.0050	23.3	0.004	0.76	39.9
0.0089	23.5	0.008	0.76	39.0
0.0147	23.3	0.014	0.76	38.1
0.0330	23.0	0.035	0.76	37.5
0.0493	23.2	0.054	0.75	37.0
0.0896	23.1	0.101	0.73	36.4
0.0980	23.3	0.115	0.74	36.0
0.0000	-	0.000	0.79	-
0.0050	23.4	0.003	0.48	48.6
0.0089	23.2	0.006	0.49	48.0
0.0192	23.3	0.014	0.48	45.3
0.0501	23.3	0.032	0.48	43.9
0.0583	23.3	0.048	0.47	43.6
0.1005	23.0	0.087	0.46	43.7
0.0000	-	0.000	0.46	-

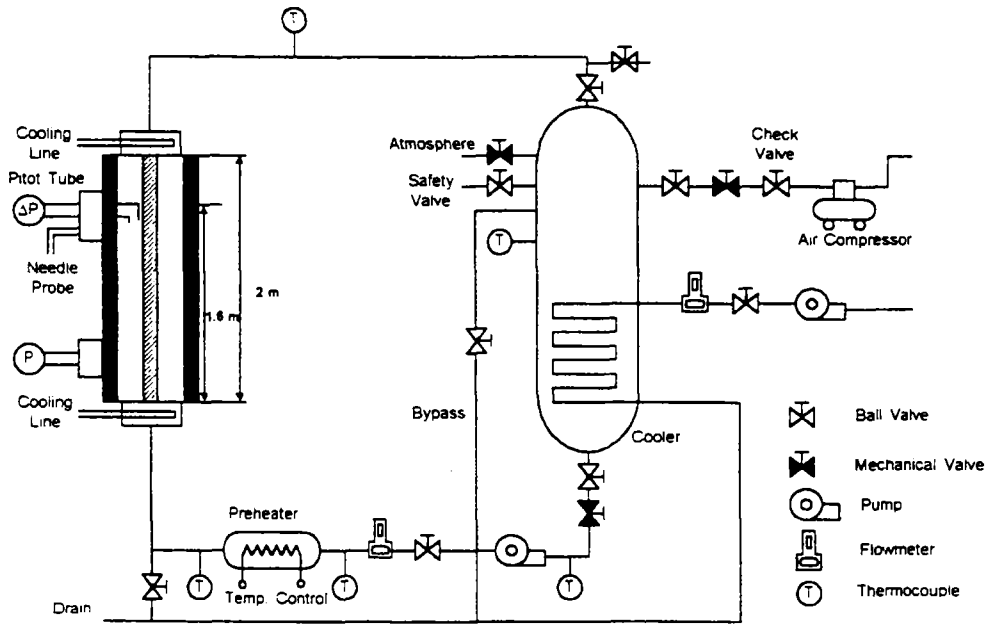

Fig. 1 Schematic Diagram of the Test Loop

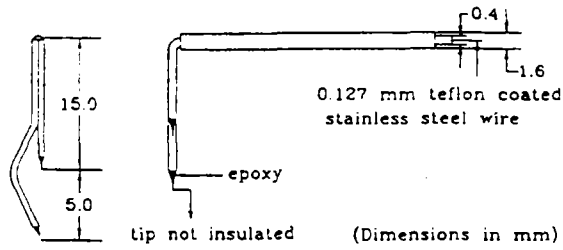

Fig. 2 Schematic Diagram of the Two-Conductivity Probe

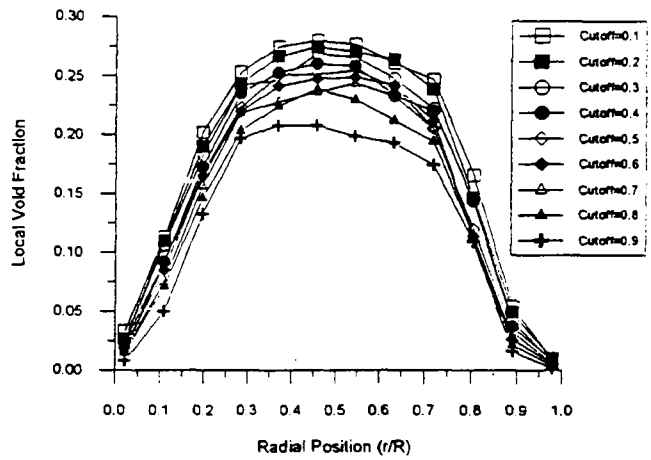

Fig. 3. Typical Variation of Void Distribution with the Cutoff in the Circular Loop

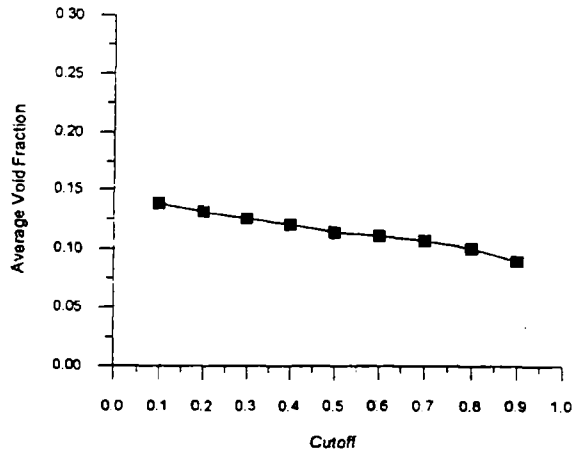

Fig. 4. Typical Variation of Average Void Fraction in the Circular Loop

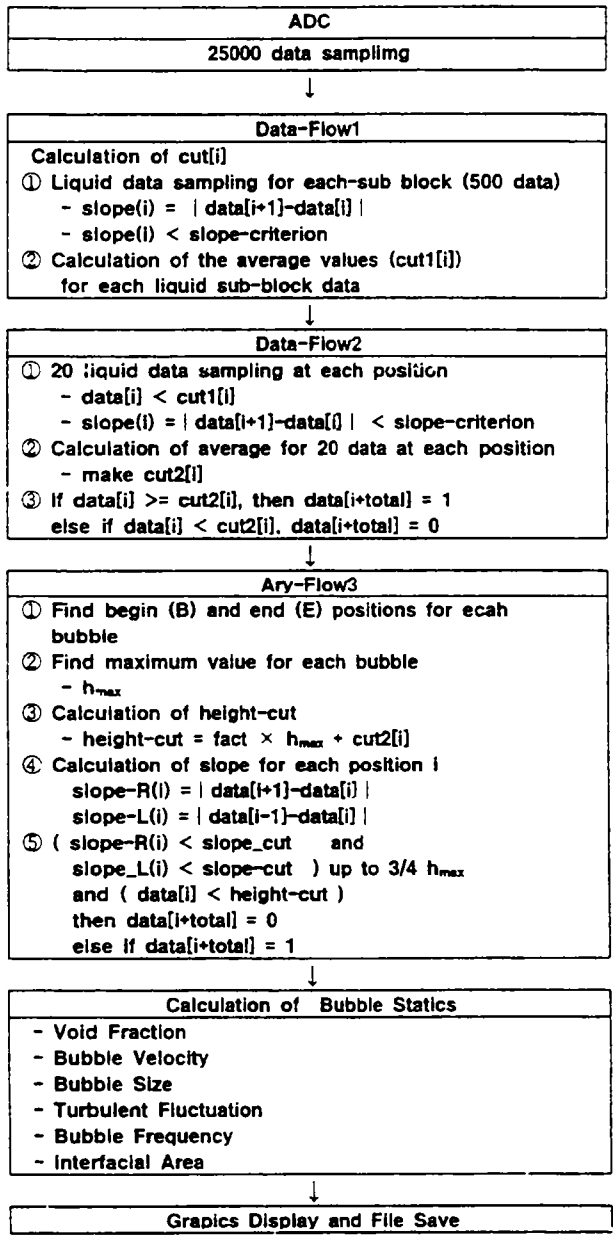

Fig. 5 Signal Processing Algorithm for the Two-Conductivity Probe

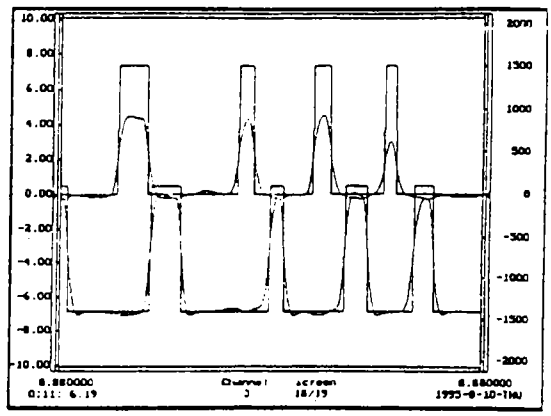

Fig. 6 Comparison of the Signal from Two-Conductivity Probe and Signal Modified by Phase Discrimination Algorithm

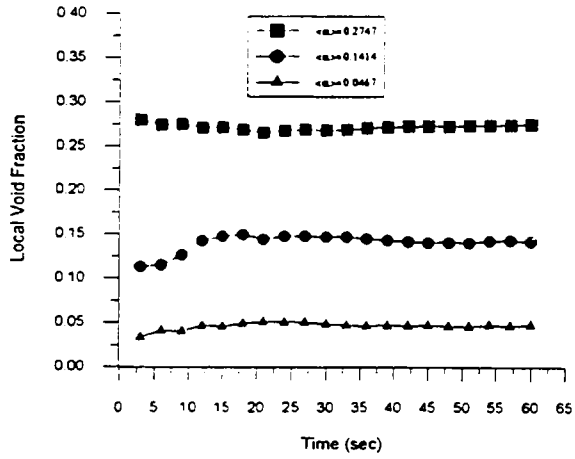

Fig. 7. Variation of Local Void Fraction with the Total Mesauring Time

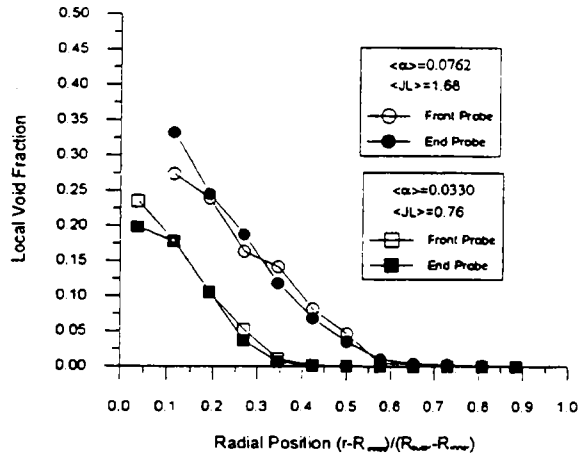

Fig. 8. Comparison of Local Void Fractions from Front and End Probes

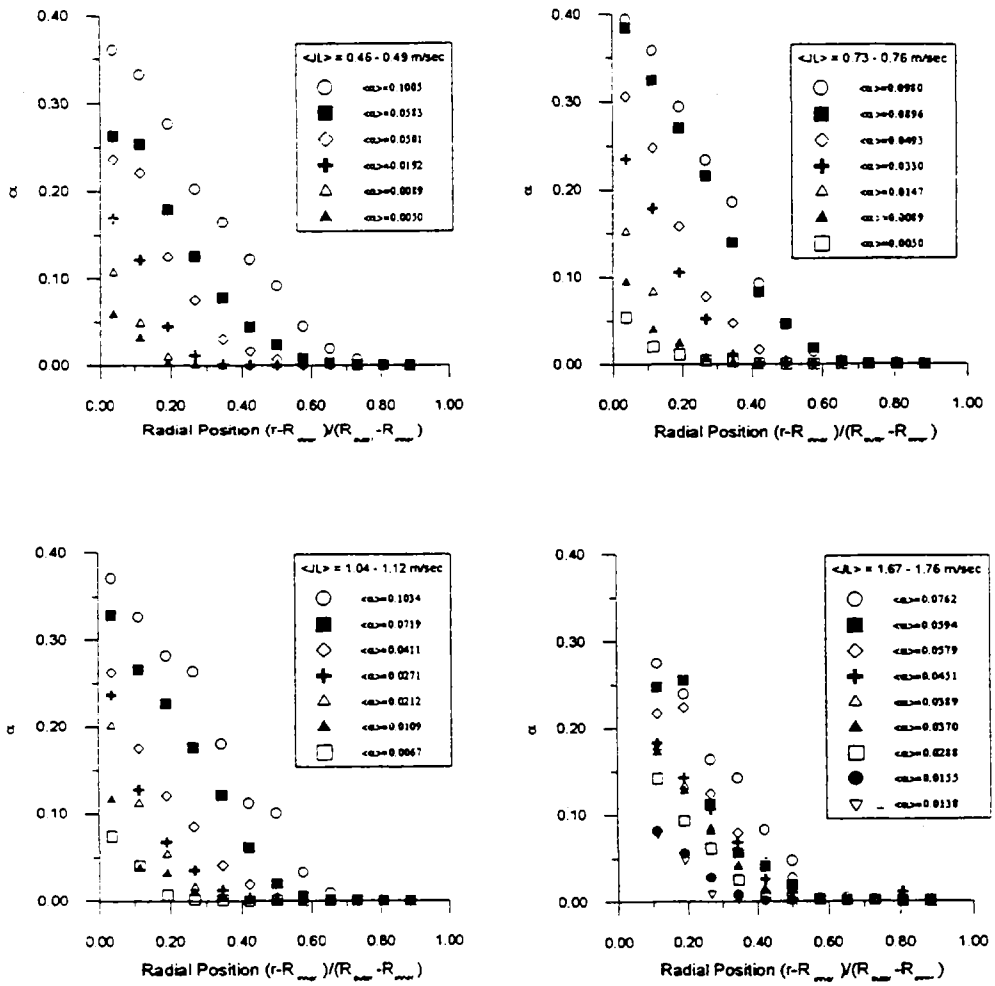

Fig. 9. Radial Distributions of Local Void Fraction in the Annulus Loop

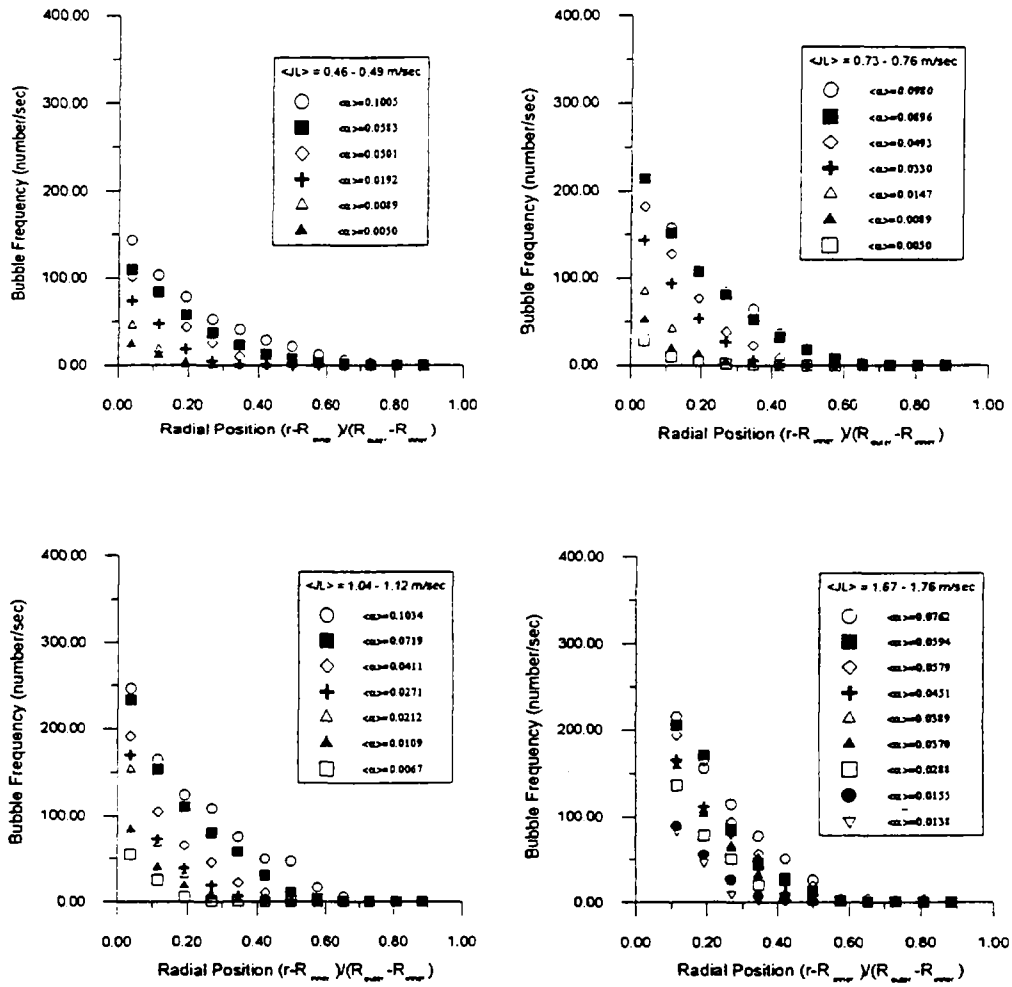

Fig. 10. Radial Distributions of Local Bubble Frequency in the Annulus Loop

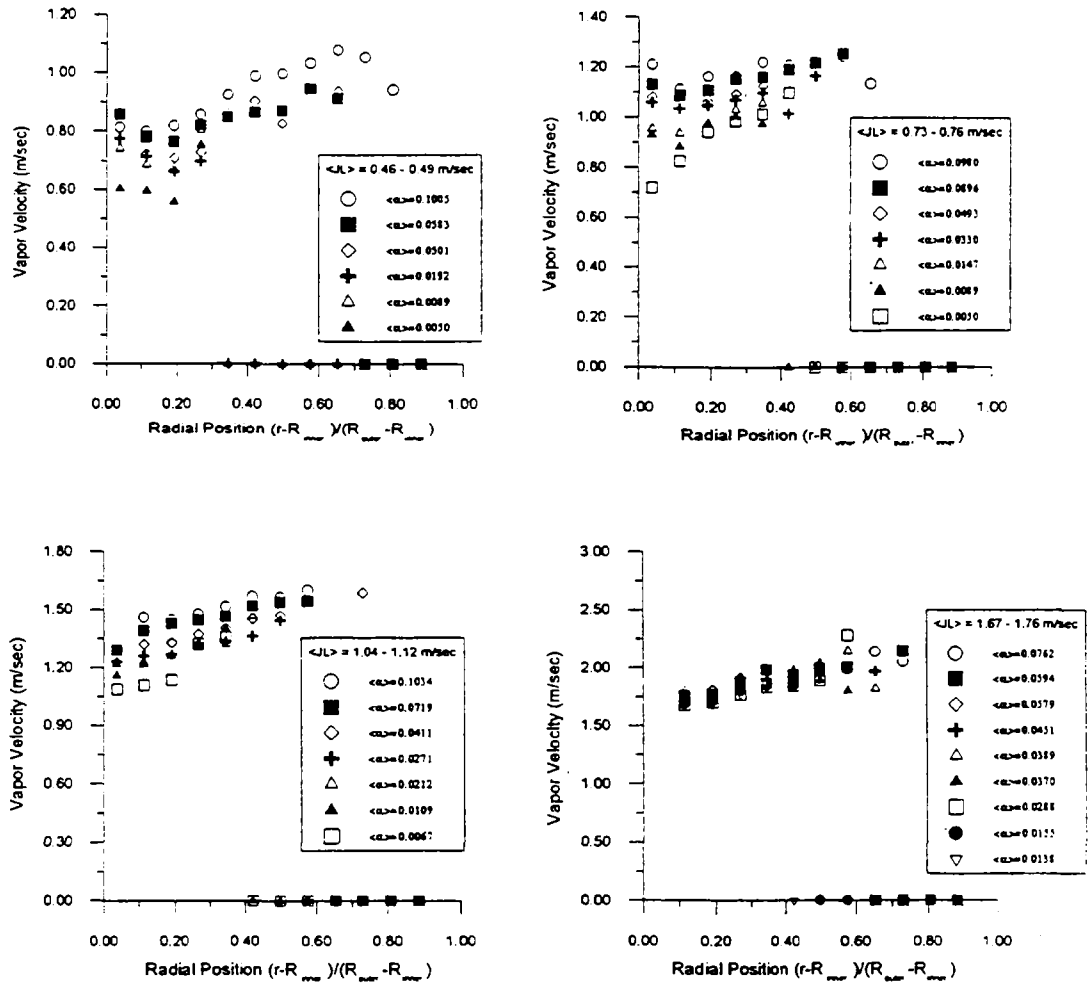

Fig. 11. Radial Distributions of Local Vapor Velocity in the Annulus Loop

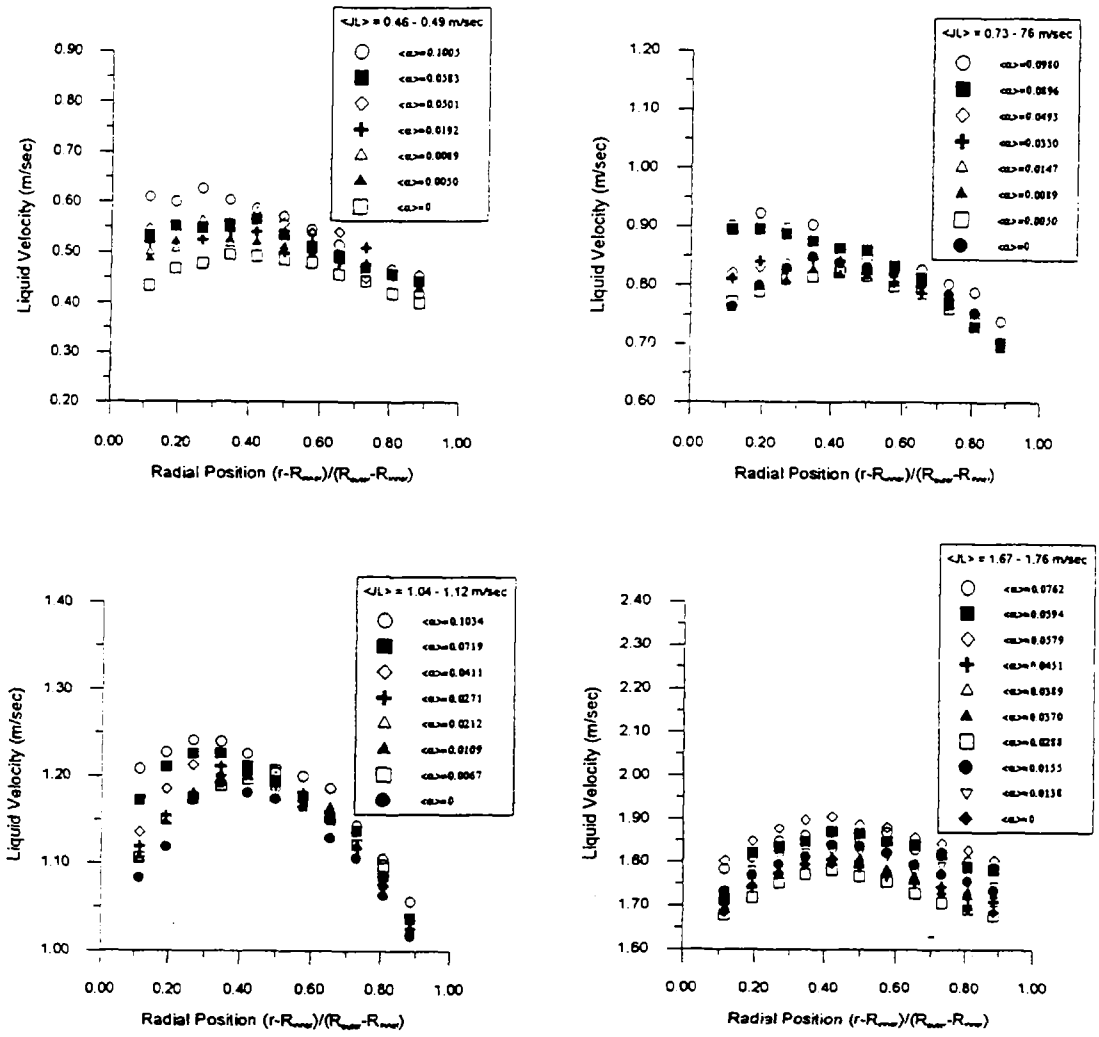

Fig. 12. Radial Distributions of Local Liquid Velocity in the Annulus Loop

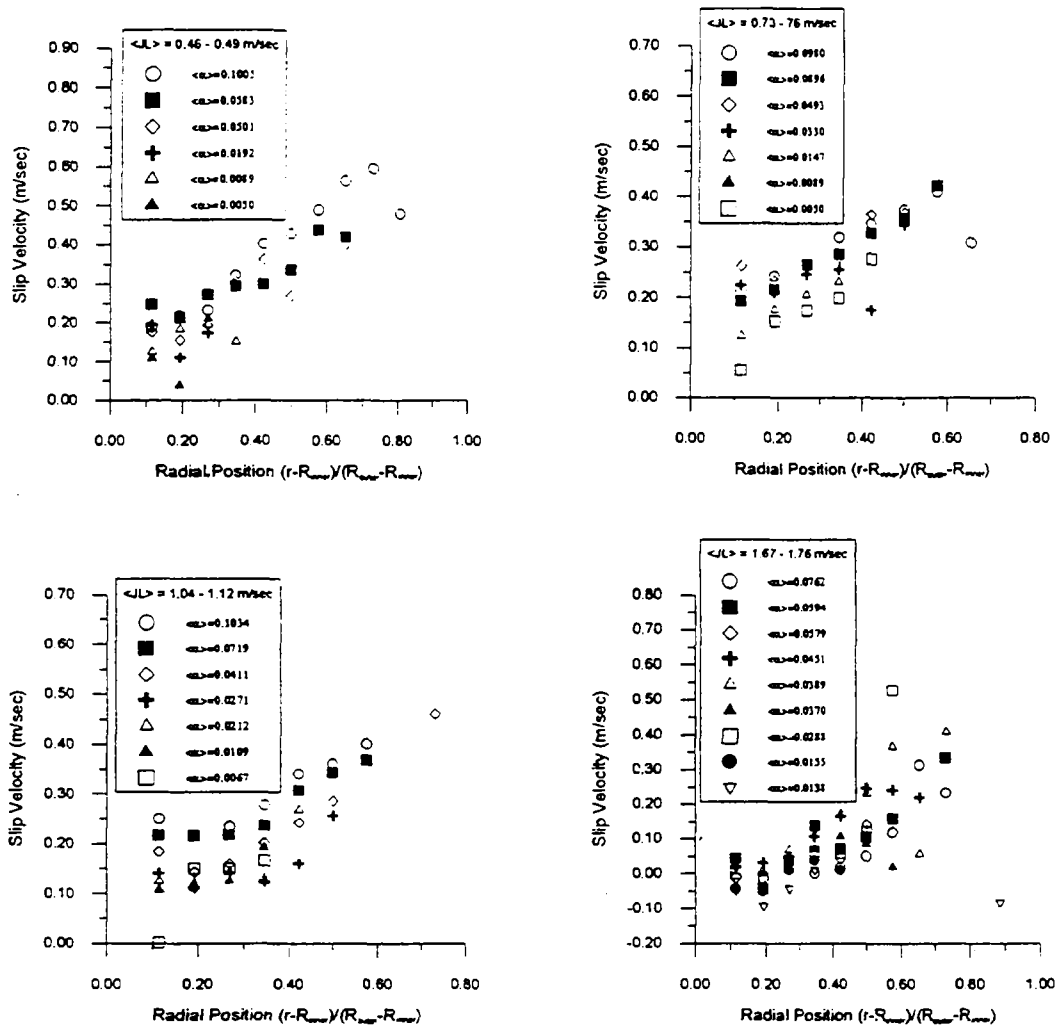

Fig. 13. Radial Distributions of Local Slip Velocity in the Annulus Loop

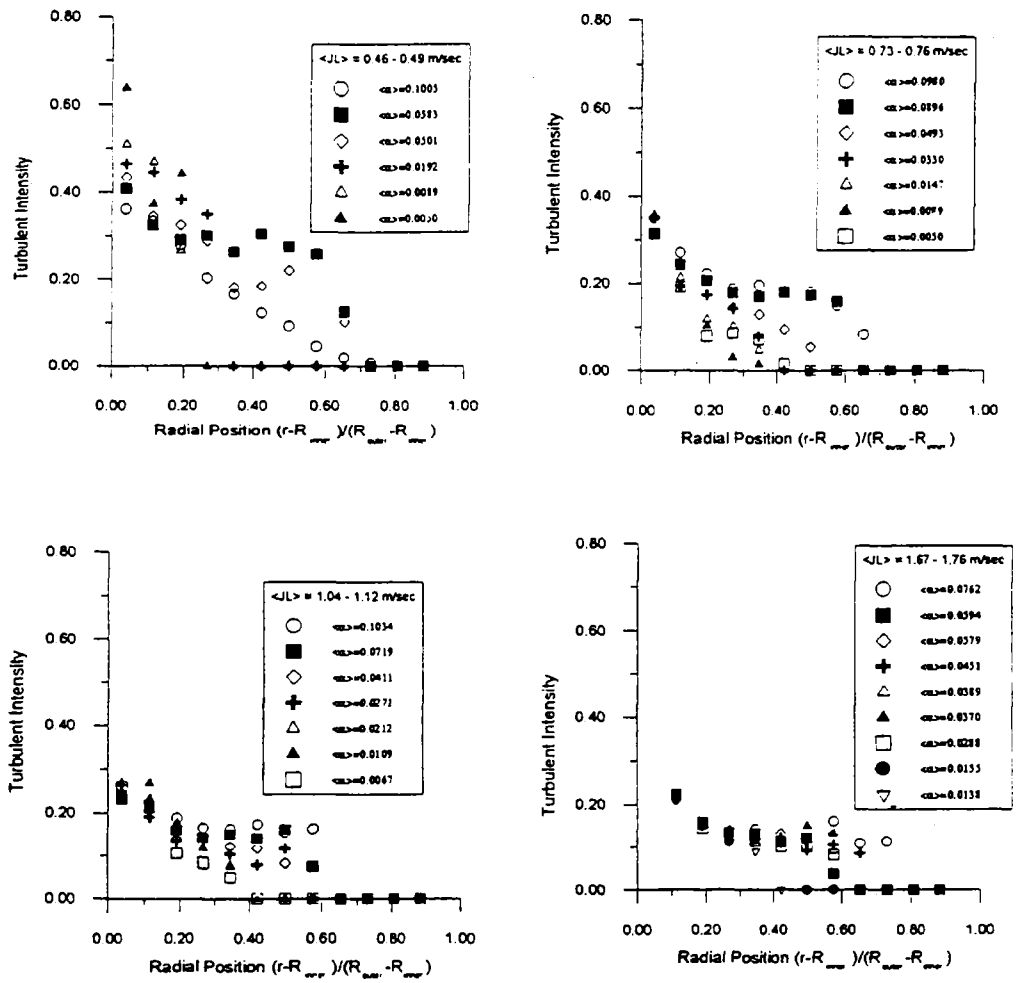

Fig. 14. Radial Distributions of Local Bubble Turbulent Fluctuation in the Annulus Loop

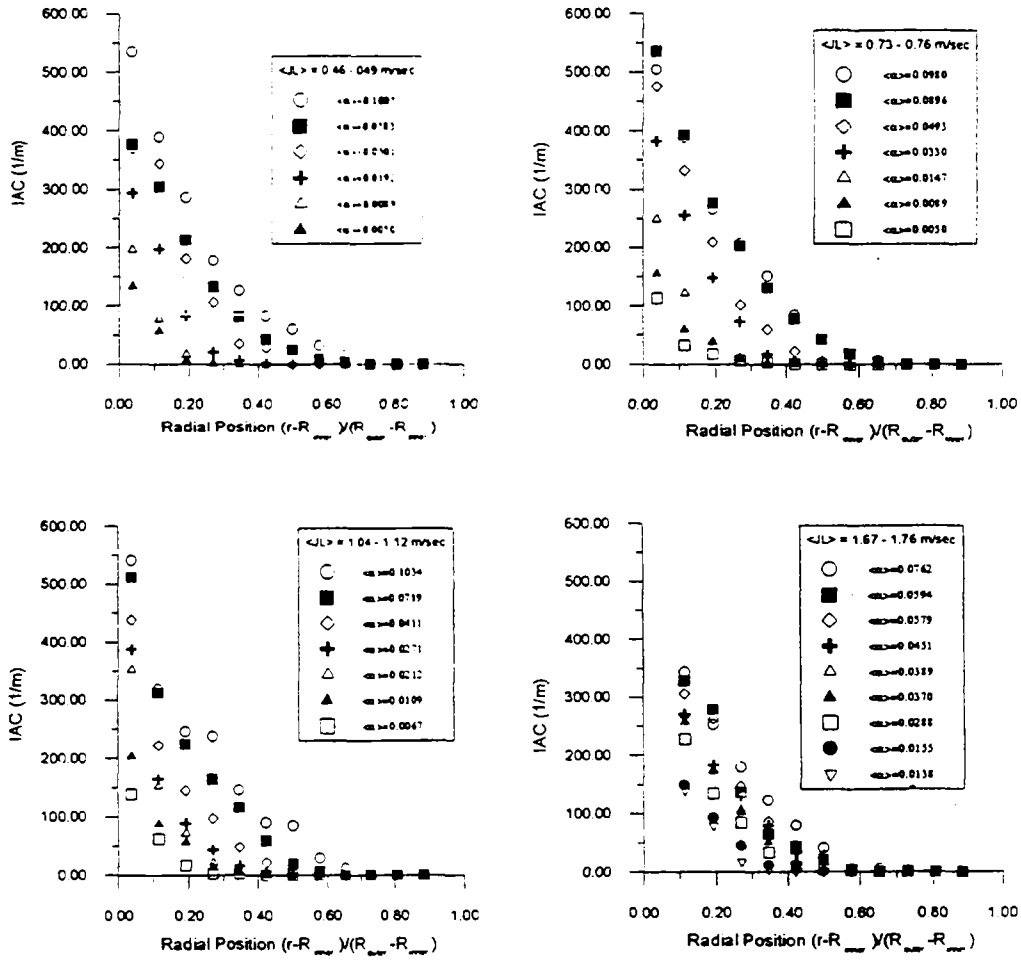

Fig. 15. Radial Distributions of Local Interfacial Area Concentration in the Annulus Loop

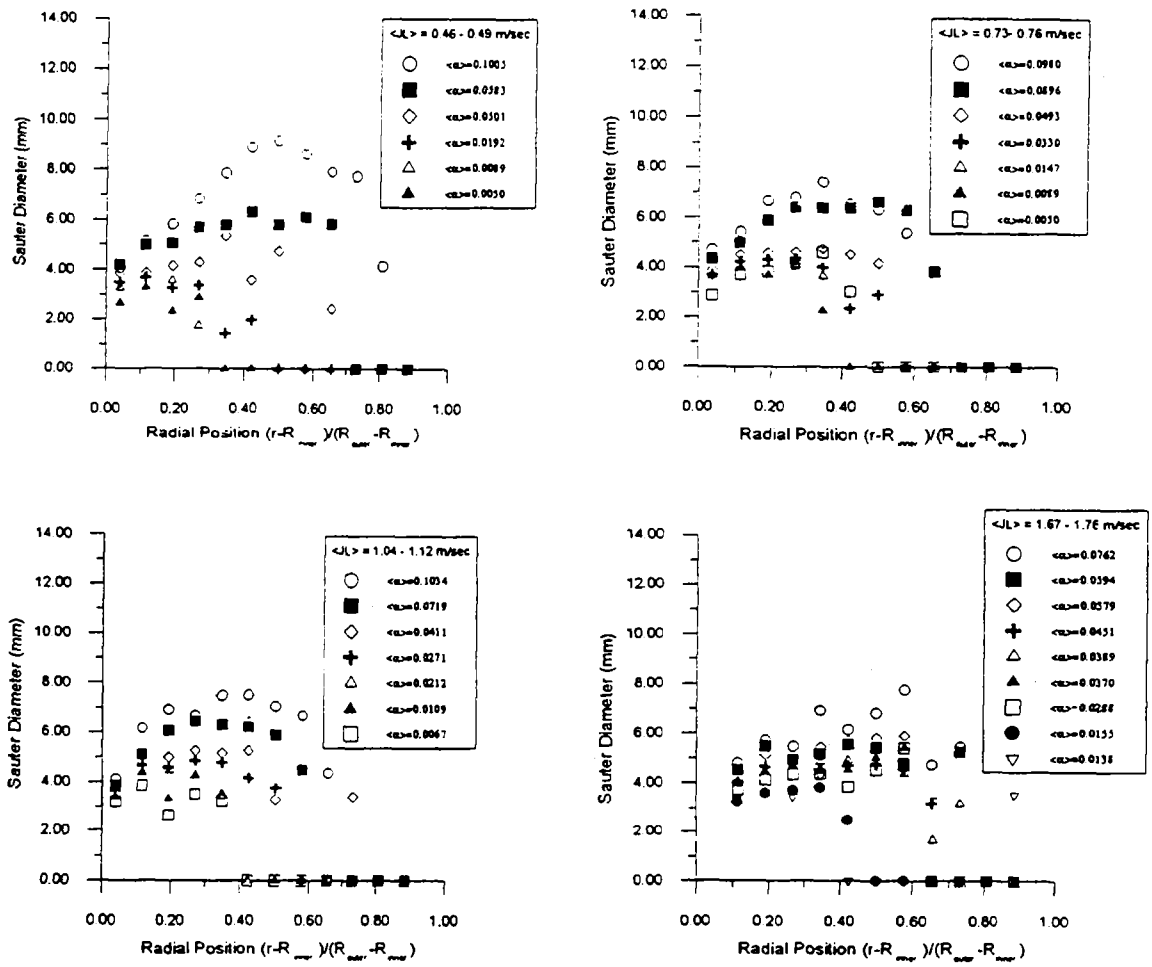

Fig 16. Radial Distributions of Local Sauter Diameter in the Annulus Loop